

Supporting Information

## **Facile Preparation of 3D Porous Agar-based Carbon Aerogels Heteroatom Doping Used in High-Energy Density Supercapacitors**

Kaijun Xie‡, Kai Xia‡, Xin Ding\*, Long Fang, Xin Liu, Xiaodong Zhang\*

College of Chemistry and Chemical Engineering, Qingdao University, Qingdao 266071, China

\*Corresponding author: dingxin@qdu.edu.cn, zhangxdqd@hotmail.com.

‡These authors contributed equally to this work.

## **Experimental sections**

### **Material preparation**

Agar, Pectin and Tamarind was obtained from Aladdin. One of them is the storage environment, which is kept at ambient temperature and in a dry atmosphere. All other chemicals were purchased from Sinopharm Chemical Reagent Co., Ltd. All chemicals were used as received. In a water bath at 90°C, heat the agar (6g) and deionized water (300g) and stir, adding water at least three times during this time and keeping the liquid level near 300mL. Meanwhile, pectin porous carbon (PPC) and tamarind porous carbon (TPC) were also synthesized in the same approach. To begin, the dissolved agar is poured into a pre-formed mold and allowed to cool to room temperature. Second, cross-link and agglomerate the agar molecules, then place the agar in the refrigerator to cool overnight. After that, it's time to freeze-dry for 48 hours.

### **Construction of Nitrogen/Oxygen Double-doped Hierarchical Porous Carbon**

Pre-treat the agar before pyrolysis in a self-made tube furnace. It was heated to 800°C at a rate of 4°C/min and then pyrolyzed at that temperature for two hours using a 1:1 mixture of NH<sub>3</sub> and N<sub>2</sub>. NH<sub>3</sub> and N<sub>2</sub> gas each flowed at a rate of 10 mL/min. The mixed gas of NH<sub>3</sub> and N<sub>2</sub> was supplied continuously for 30 minutes after the temperature was raised to 800°C. To maintain a steady flow rate, NH<sub>3</sub> is turned off and just N<sub>2</sub> is pumped on. APC is the name for the sample received. Preparing pectin and tamarind follows the same steps. PPC and TPC are the abbreviations for the two types of compounds. PPC and TPC were pyrolyzed at appropriate temperatures for comparison.

### **Material Characterization**

Scanning electron microscopy (SEM, GeminiSEM 500) and transmission electron microscope (TEM, JEOL 2100f) were used to examine the morphology of the produced electrode material. Cu K $\alpha$  radiation X-ray diffractometer was utilized by XRD (Rigaku, Ultima IV) to determine the crystal properties of the sample. A DXR 2xi spectrometer was used to detect the Raman spectrum at a wavelength of 532 nm. The nitrogen adsorption/desorption BET (ASAP2460) technique was used to determine the sample specific surface area, and the density functional theory (DFT) model was used to quantify the sample pore size distribution. The ESCALAB 250Xi spectrometer collects data using a monochromatic (K $\alpha$  radiation) source. The thermogravimetric analyzer TG/DSC NETZSCH STA 449F3 in N<sub>2</sub> at 30°C to 700°C performs thermogravimetric analysis (TGA).

### **Electrochemical characterization**

In a nitrogen methyl pyrrolidone solution, combine 80% electrode material, 10% carbon black, and 10% polytetrafluoroethylene completely, then apply it to a foamed nickel of 1cm\*1cm and dry it in the oven. Working electrodes, reference electrodes, and counter electrodes are made up of nickel foam, Hg/HgO electrode, and platinum sheet filled with electrode materials. In a three-electrode setup with a 6 M KOH aqueous solution, the electrochemical performance of a single electrode was investigated. In a voltage window of -1-0V, test the CV curve of a single electrode at different scan speeds. Carry out the constant current charge and discharge test in the same voltage window, and monitor the GCD change throughout a current density range of 0.5 to 20 A g<sup>-1</sup>. The open circuit potential of electrochemical impedance spectroscopy (EIS, Nyquist diagram) is 5 mV s<sup>-1</sup>, with a frequency range of 0.01 Hz to 100 kHz. To create a symmetrical capacitor, two APC electrode materials of equal quality (both positive and negative electrodes are composed of APC electrode materials) are chosen and separated by a glass fiber separator. For electrochemical testing, the whole system was submerged in a 1M Na<sub>2</sub>SO<sub>4</sub> aqueous solution. An electrochemical workstation was used to conduct all of the electrochemical experiments at room temperature(CHI 760E, CH Instruments, Inc.).

The gravimetric specific capacitance (C) was calculated using the following equations:

$$C = \frac{I\Delta t}{m\Delta V} \quad (1)$$

$$C = \frac{\int IdV}{vmV} \quad (2)$$

where I is the current density, ΔV is the potential change within the discharge time Δt, V is potential, v is the potential scan rate, and m is the mass of the electroactive materials. (capacitance unit: Fg<sup>-1</sup>)

The gravimetric specific capacity, energy density (E) and power density (P) of the symmetric system were computed by the formula:

$$E = \frac{CV^2}{2} = \frac{C_p \Delta U^2}{7.2} \quad (3)$$

$$P = \frac{E}{\Delta t} = \frac{E * 3600}{\Delta t} \quad (4)$$

Where I is the current density, V is the working range, v is the scan rate, m is the weight of the active materials of the two electrodes and Δt is the discharge time (s). (Energy density unit: Wh Kg<sup>-1</sup>, Power density unit: W Kg<sup>-1</sup>)

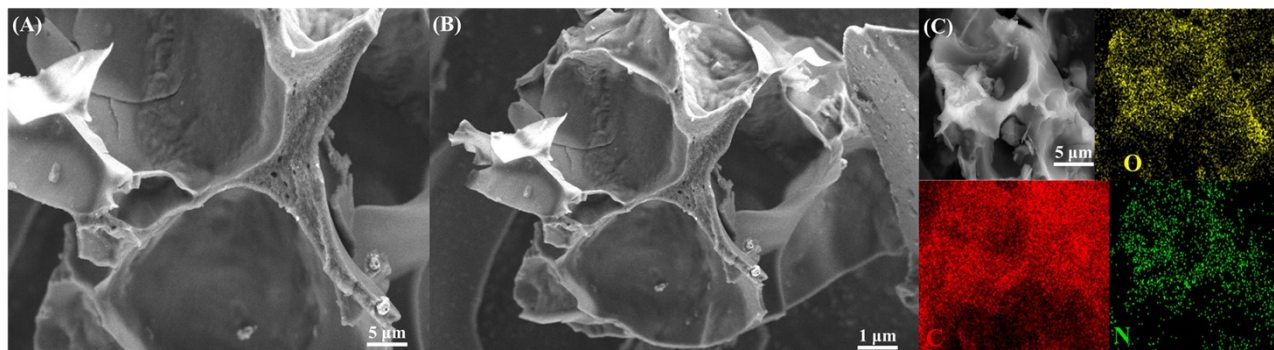
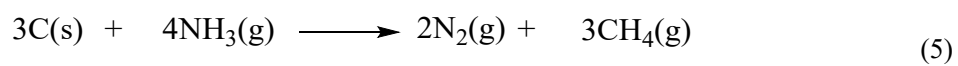


**Figure S1.** (A), (B) SEM images of PPC. (C) EDS elemental mapping images of C, N, and O in PPC, respectively.

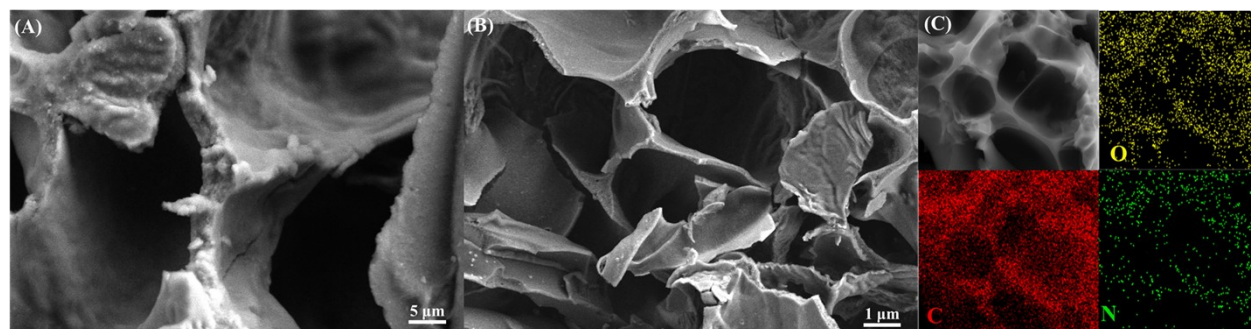


**Figure S2.** (A), (B) SEM images of TPC. (C) EDS elemental mapping images of C, N, and O in TPC, respectively.

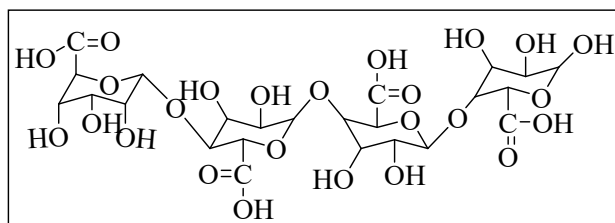


**Figure S3** Pectin

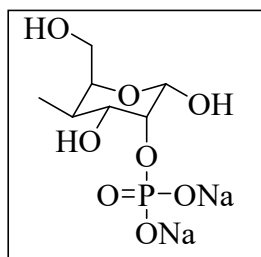


**Figure S4** Tamarind

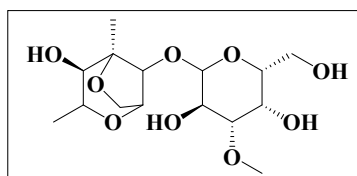


**Figure S5** Agar

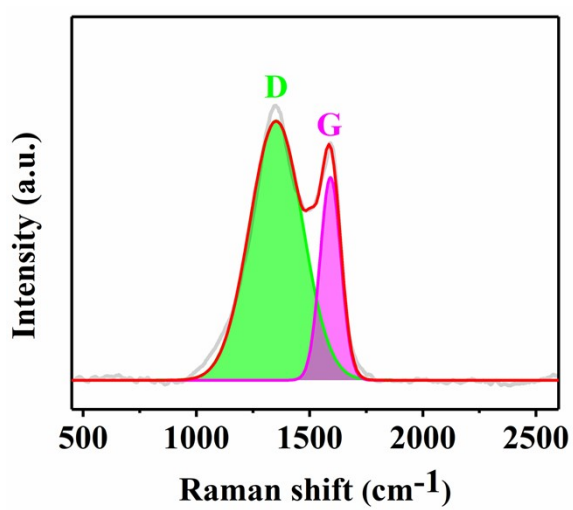


**Figure S6** Raman spectrum of APC

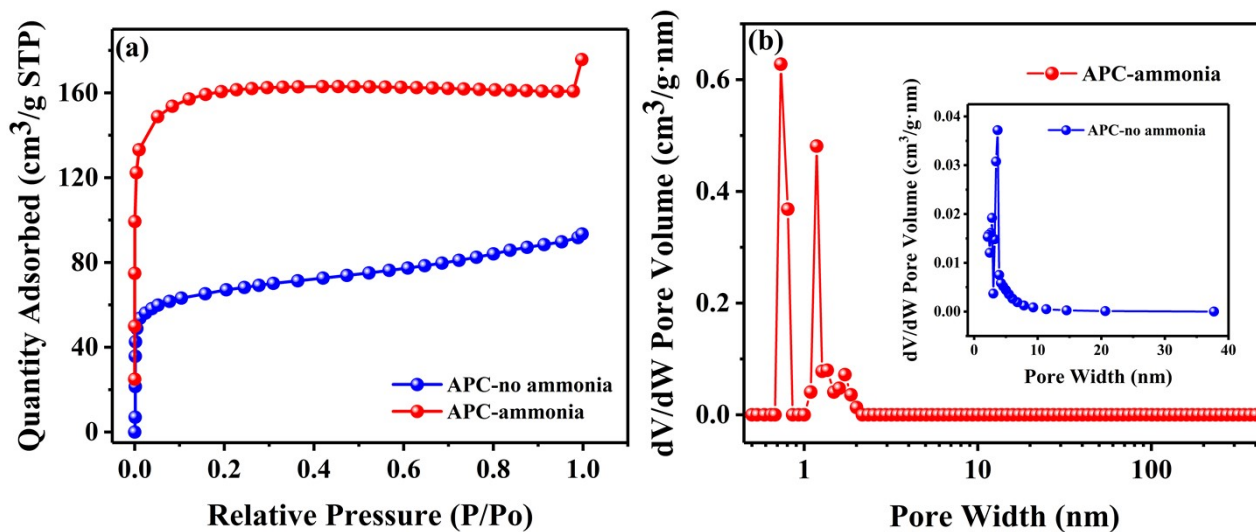


**Figure S7.** (a) the adsorption isotherm of 2% agar porous carbon impermeable to ammonia and ammonia. (b) the pore size distribution diagram of 2% agar porous carbon impermeable to ammonia and ammonia

**Table 1S** Physical parameters of as-prepared carbon materials.

Samples	$V_{total}$ ( $\text{cm}^3 \text{g}^{-1}$ )	$V_{mic}$ ( $\text{cm}^3 \text{g}^{-1}$ )	$V_{ext}$ ( $\text{cm}^3 \text{g}^{-1}$ ) <sup>b</sup>	$S_{BET}$ ( $\text{m}^2 \text{g}^{-1}$ ) <sup>d</sup>	$S_{mic}$ ( $\text{m}^2 \text{g}^{-1}$ ) <sup>e</sup>	$S_{ext}$ ( $\text{m}^2 \text{g}^{-1}$ ) <sup>f</sup>	$D$ (nm) <sup>g</sup>
PPC	0.144	0.126	0.018	278.23	260.57	17.66	2.06
APC	0.271	0.238	0.033	513.33	492.52	20.81	2.08
TPC	0.171	0.164	0.007	342.07	334.59	7.48	1.99
APC- ammonia	0.271	0.238	0.033	513.33	492.52	20.81	2.08
APC-No ammonia	0.145	0.071	0.074	216.12	142.27	73.85	2.13

<sup>a</sup> Total pore volume ( $V_{total}$ ) was estimated from the adsorbed amount at a relative pressure of 0.99.

<sup>b</sup> Micropore volume ( $V_{mic}$ ) was obtained from  $t$ -plot method.

<sup>c</sup> External pore volume ( $V_{ext}$ ) was obtained from  $t$ -plot method ( $V_{ext} = V_{total} - V_{mic}$ ).

<sup>d</sup> Specific surface area ( $S_{BET}$ ) was calculated with modified Brunauer-Emmett-Teller (BET) method.

<sup>e</sup> Micropore surface area ( $S_{mic}$ ) was obtained from  $t$ -plot method.

<sup>f</sup> External pore volume ( $S_{ext}$ ) was obtained from  $t$ -plot method ( $S_{ext} = S_{BET} - S_{mic}$ ).

<sup>g</sup> Average pore diameter ( $D$ ) was obtained from  $D = 4 V_{total}/S_{BET}$ .

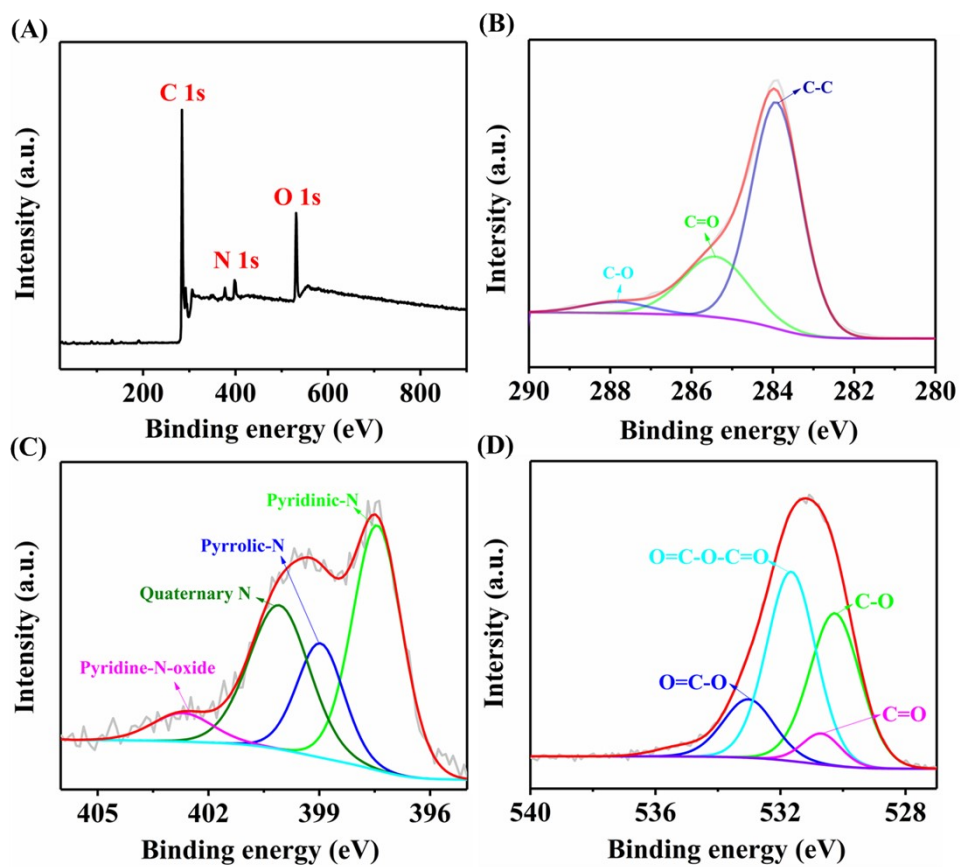


**Figure S8.** (A) XPS survey spectrum of PPC, high-resolution spectrum of PPC. (B) C 1s, (C) N 1s and (D) O 1s spectra of PPC.

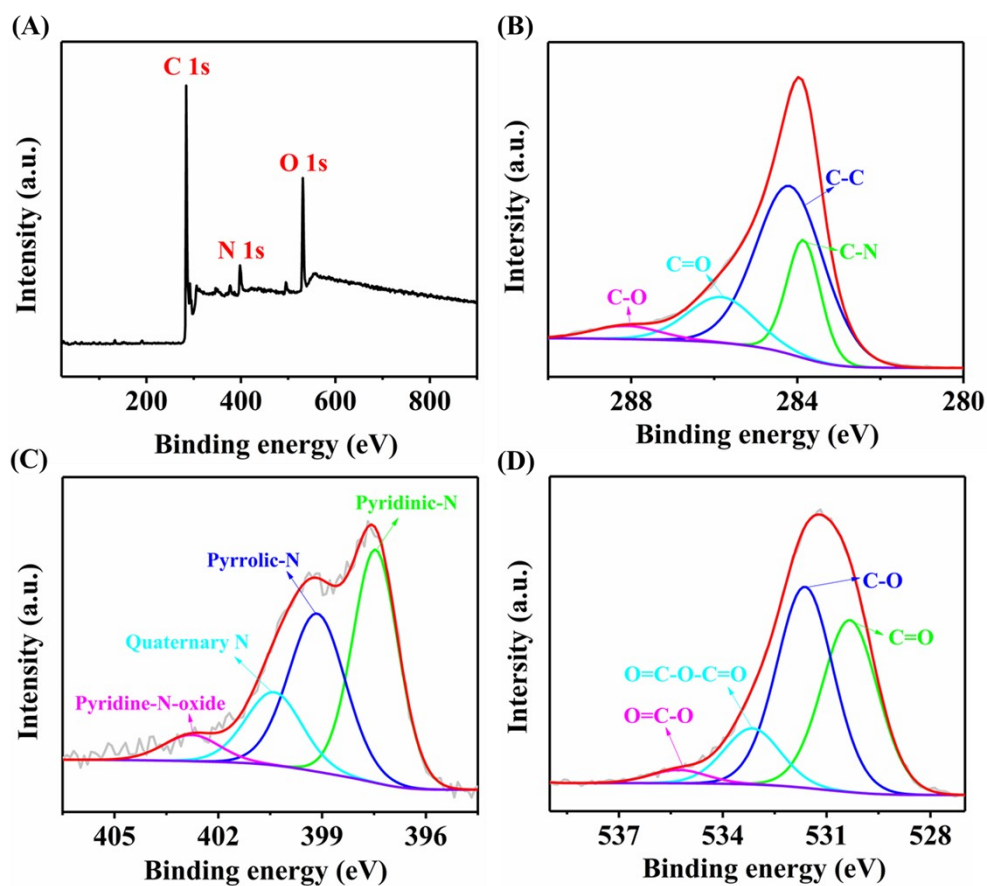


**Figure S9.** (A) XPS survey spectrum of TPC, high-resolution spectrum of TPC. (B) C 1s, (C) N 1s and (D) O 1s spectra of TPC.

**Table 2S** The atomic percentages of C, O, and N in carbon materials as determined by XPS findings, as well as the yield of porous carbon attained at various temperatures.

Samples	Yield (%)	C at%	O at%	N at%
APC	22.3%	85.11	9.56	5.33
PPC	17.9%	87.13	9.79	3.08
TPC	10.8%	88.35	10.23	1.42

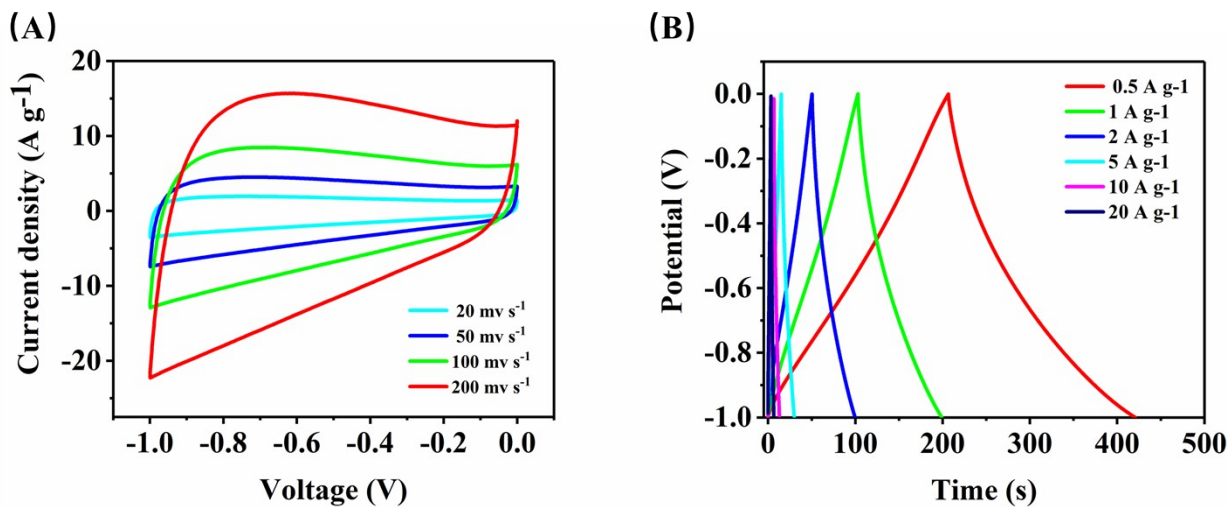


**Figure S10.** (A) CV curves of PPC at different scan rates of 20-200 mV s<sup>-1</sup> in 6.0 M KOH aqueous solution. (B) Galvanostatic charge/discharge curves of the PPC at various current densities.

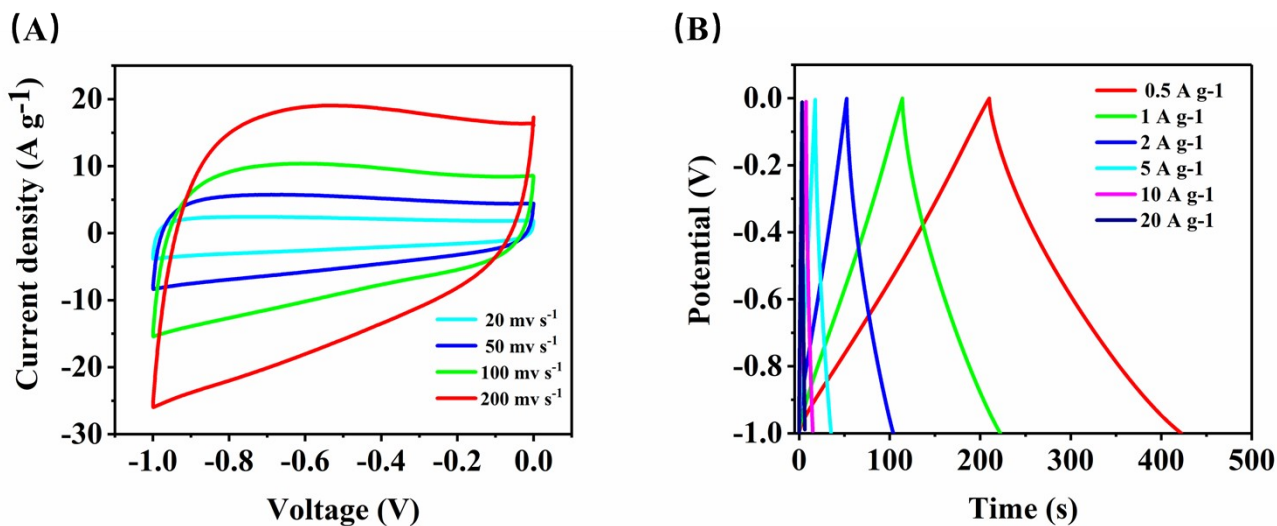


**Figure S11.** (A) CV curves of TPC at different scan rates of 20-200 mV s<sup>-1</sup> in 6.0 M KOH aqueous solution. (B) Galvanostatic charge/discharge curves of the TPC at various current densities.

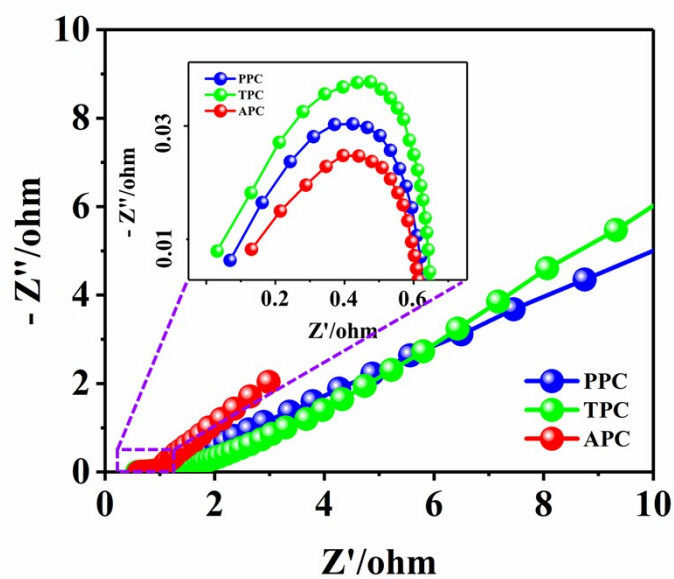


**Figure S12.** Nyquist plots of PPC, TPC and APC electrodes.

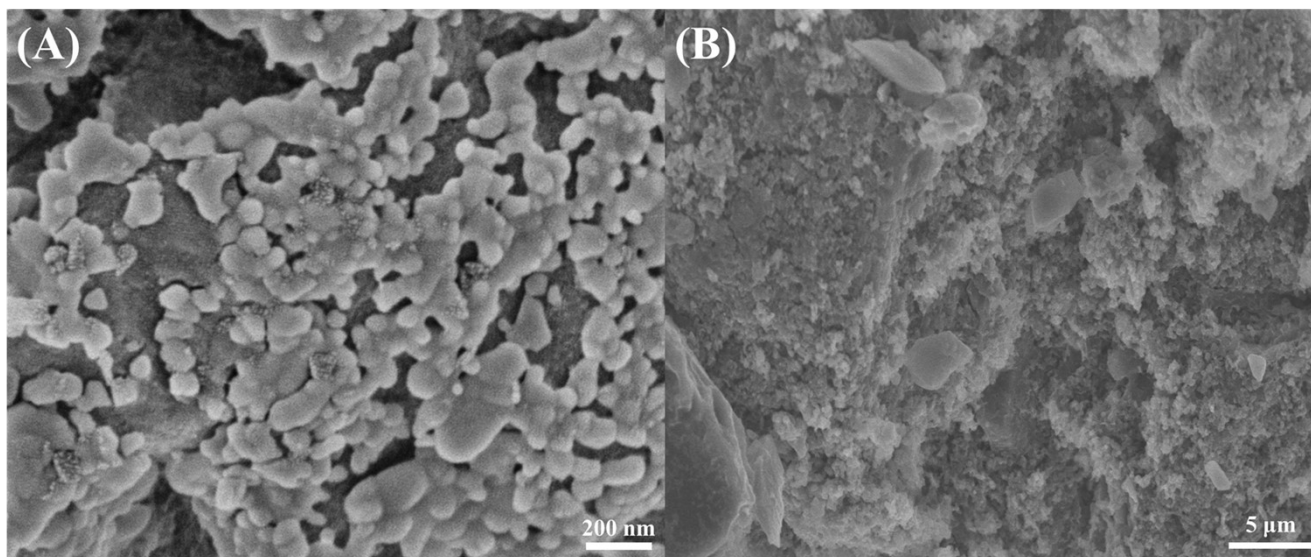


**Figure S13.** (A) SEM of APC electrode material before 10,000 cycle testing. (B) SEM of APC electrode material after 10,000 cycle tests.

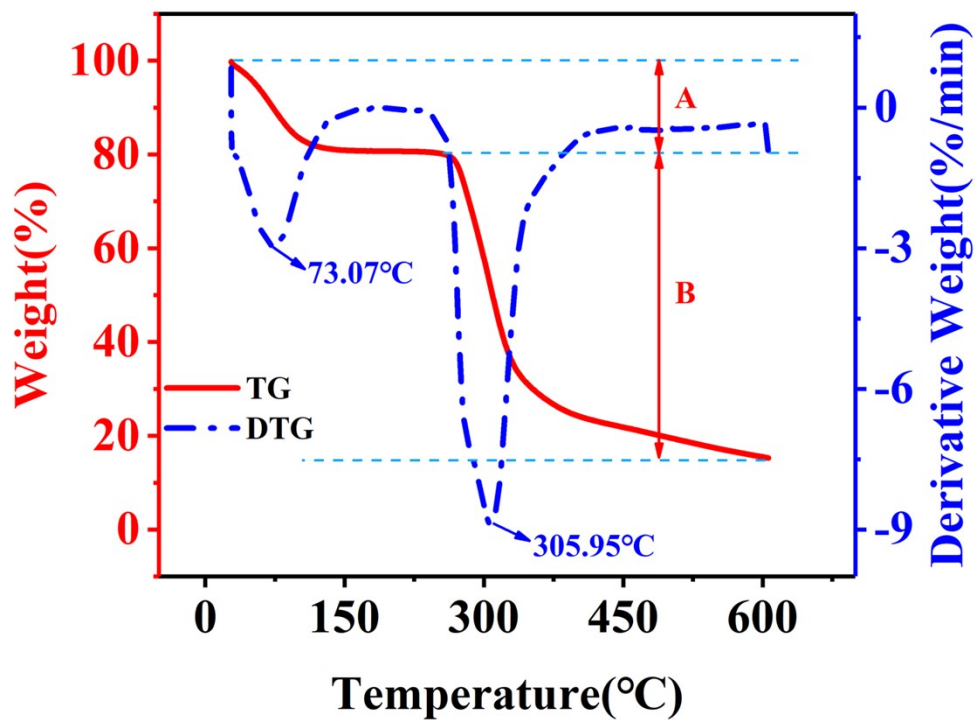


**Figure S14.** Thermogravimetric analysis (TGA) curve of agar annealed from 30-700°C under nitrogen protection. The two main weight loss stages A and B are respectively related to the desorption of water and volatile compounds and the pyrolysis of agar.

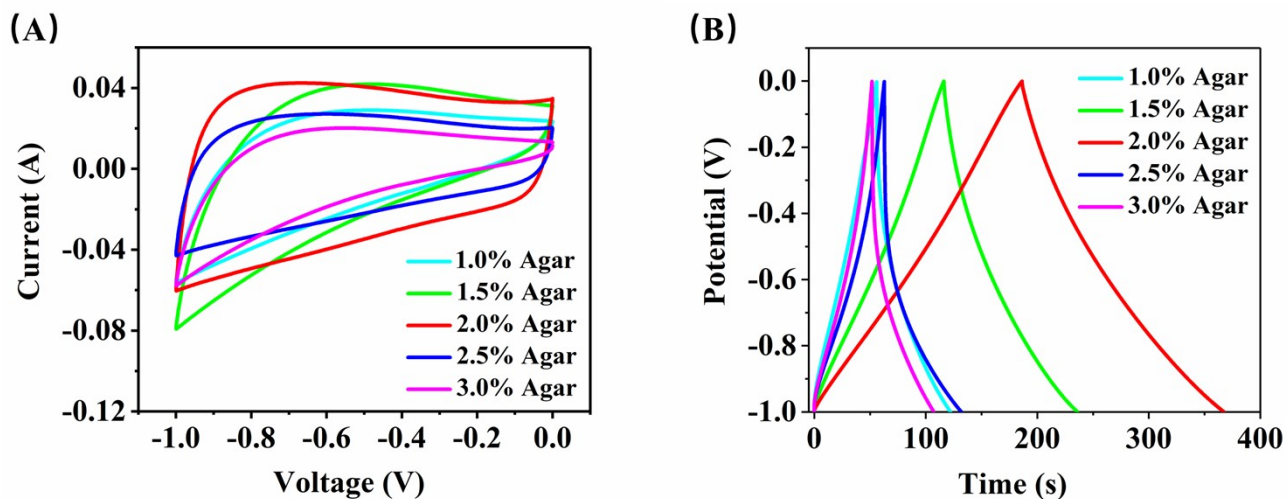


**Figure S15.** (A) CV curves of agar with different contents. (B) the GCD curves of agar with different contents.

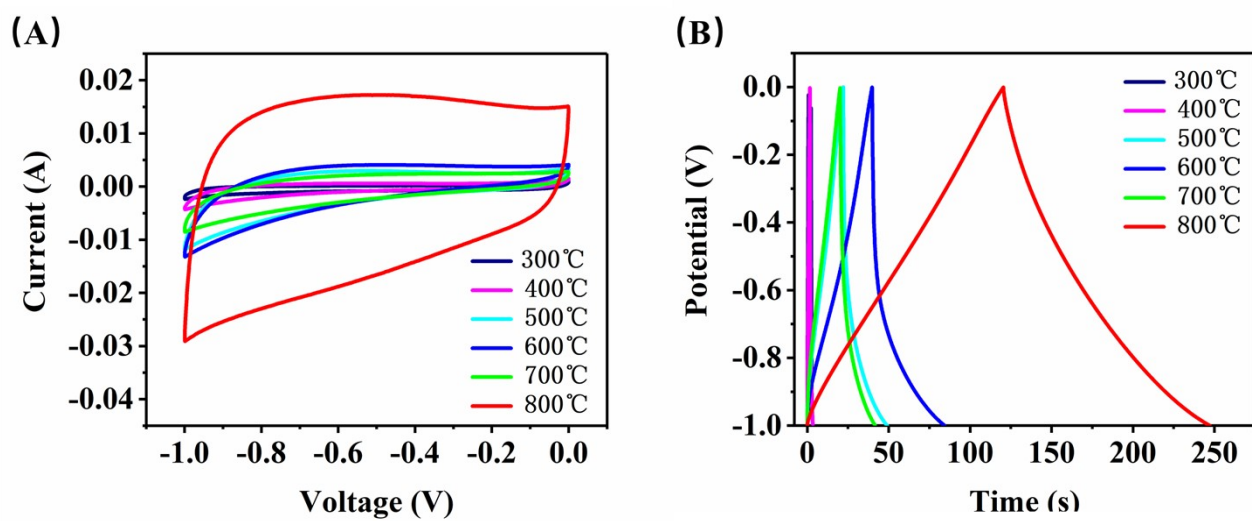


**Figure S16.** (A) the CV curves of agar at different temperatures. (B) the GCD curves of agar at different temperatures.

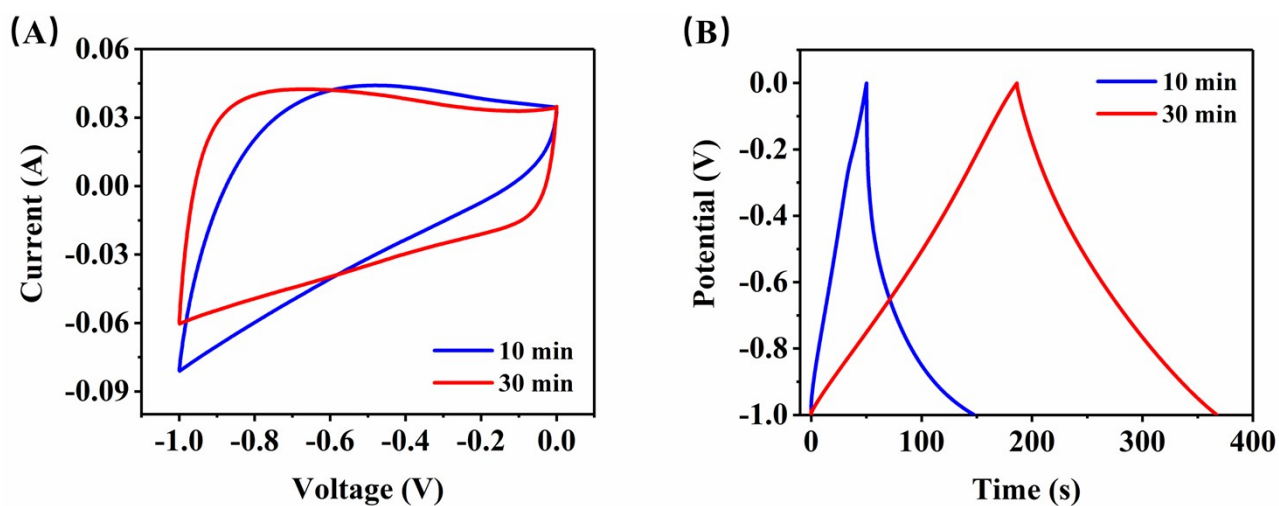


**Figure S17.** (A) the CV curve of agar with ammonia gas at different times. (B) the GCD curve of agar with ammonia gas at different times.

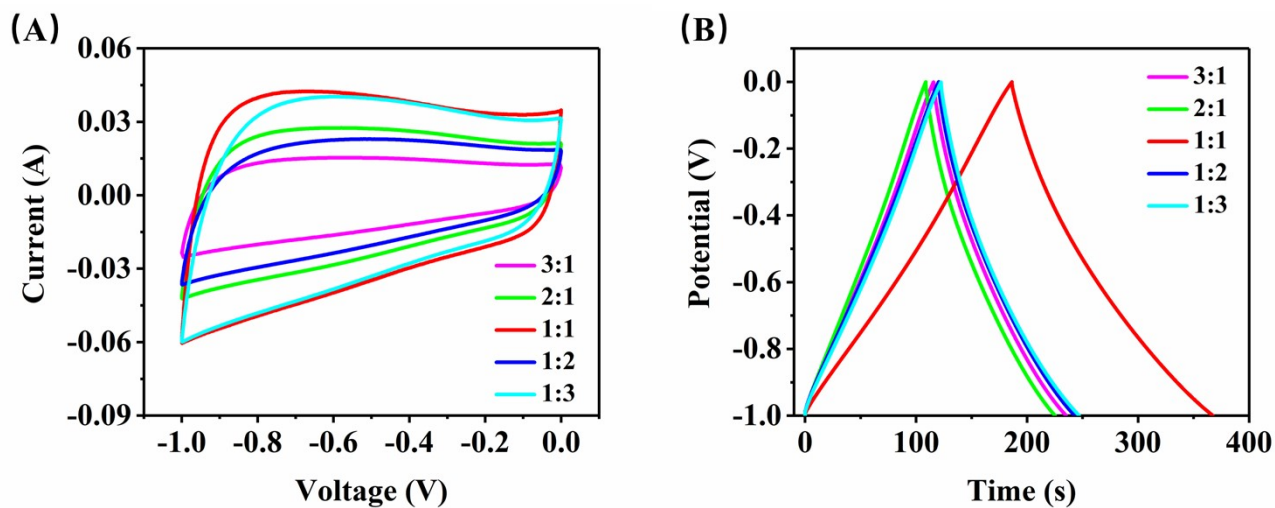


**Figure S18.** (A) the CV curve of agar under different ammonia-nitrogen ratios. (B) the GCD curve of agar under different ammonia-nitrogen ratios.

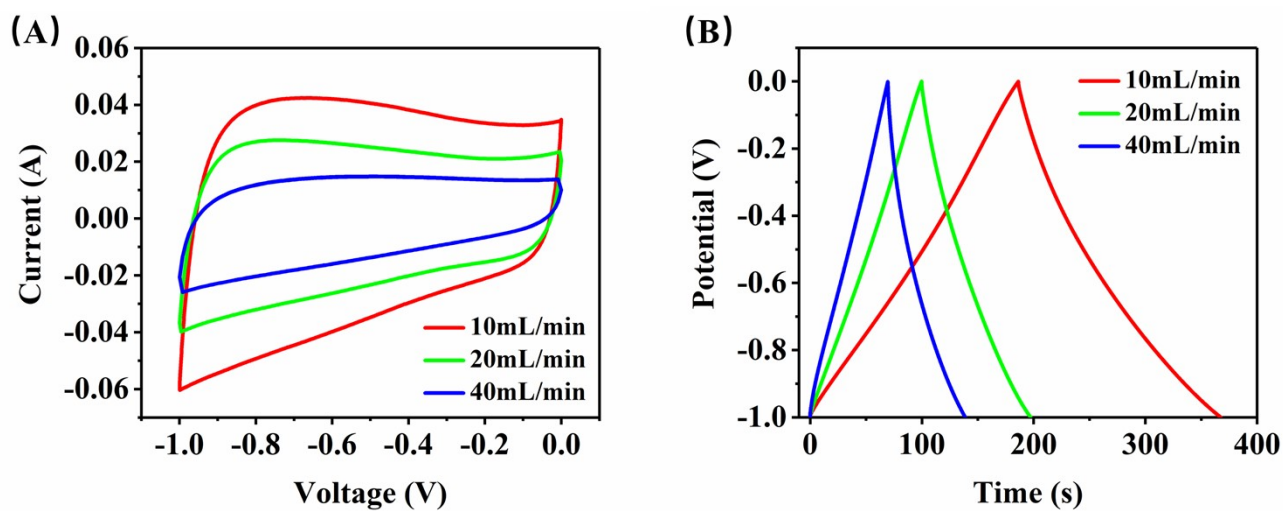


**Figure S19.** (A) the CV curve of agar with ammonia gas at different flow rates. (B) the GCD curve of agar with ammonia gas at different flow rates.

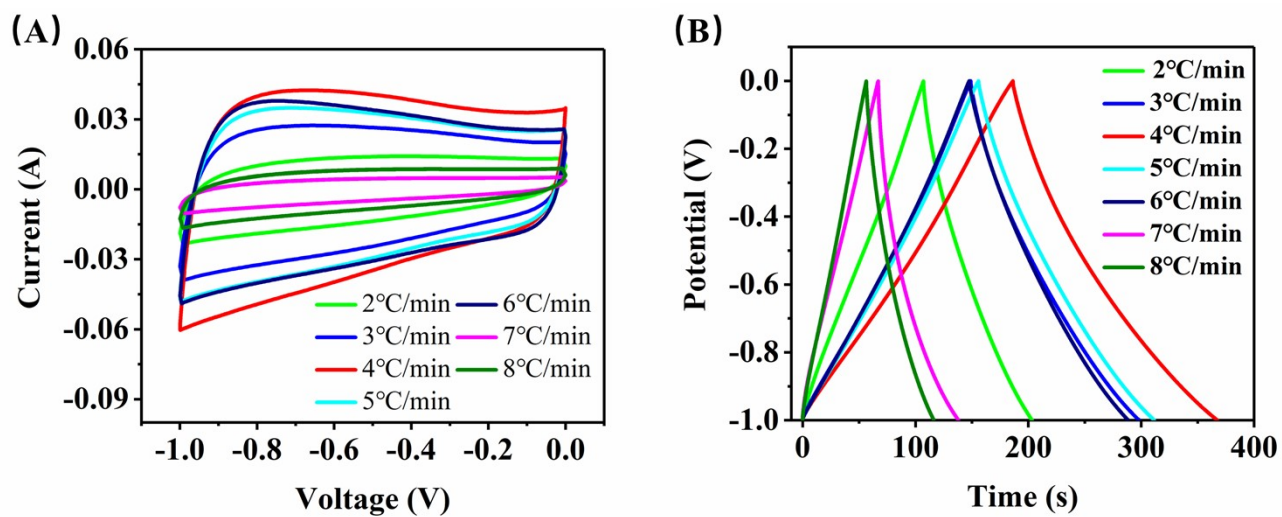


**Figure S20.** (A) the CV curve of agar at different heating rates. (B) the GCD curve of agar at different heating rates.

**Table S3.** The chemical compositions of the varied materials

	Surface Area	Raman	O	N	Energy density	Power density	Ref.
	(m <sup>2</sup> g <sup>-1</sup> )	I <sub>G</sub> /I <sub>D</sub>	(at%)	(at%)	(Wh kg <sup>-1</sup> )	(W kg <sup>-1</sup> )	
1	2090	1.14	14.12	5.3	15.9	500	[1]
2	1300	1.03	9.7	2.4	24.1	242	[2]
3	3025	2.71	7.12	4.26	15.7	325	[3]
4	1509	0.94	5.38	4.08	8.40	510	[4]
5	1054	1.35	24	2	8.6	38.9	[5]
6	2520	1.01	10.2	1.56	30.3	341	[6]
7	1770	0.86	11	5.8	10.2	100	[7]
8	1007	-	-	0.37	7.8	150	[8]
9	1091	0.98	-	6.27	9.43	630	[9]
10	716	0.94	7.0	15.6	6.2	300	[10]
11	2129	0.99	0.93	9.59	10.0	250	[11]
12	1847	0.95	42.55	0.26	11.9	463	[12]
13	-	-	16	13	11.0	166	[13]
14	474.99	0.84	16.08	-	9.345	687	[14]
15	1569	-	20.52	3.05	7.4	248	[15]
16	277.2	0.84	12.83	7.68	7.9	219	[16]
17	489.3	0.93	14.73	2.35	19.54	500	[17]
18	<b>513.3</b>	<b>1.18</b>	<b>9.56</b>	<b>6.33</b>	<b>20.4</b>	<b>449</b>	<b>This work</b>

**Table S4.** Comparison of the capacitance and energy density for previously reported carbon materials in aqueous electrolyte.

<b>Material</b>	<b>C (F g<sup>-1</sup>)</b>	<b>Electrolyte</b>	<b>Ref.</b>
Coconut shell	268 (1.0 A g <sup>-1</sup> )	6M KOH	[18]
Fallen leaves	242 (0.3 A g <sup>-1</sup> )	6M KOH	[19]
N-doped graphene aerogel	150(1.0 A g <sup>-1</sup> )	6M KOH	[20]
Carbonized cotton	207(1.0 A g <sup>-1</sup> )	1M H <sub>2</sub> SO <sub>4</sub>	[21]
D-Glucosamine	213(0.5 A g <sup>-1</sup> )	6M KOH	[22]
N-doped graphene	226(2.0 A g <sup>-1</sup> )	1M H <sub>2</sub> SO <sub>4</sub>	[23]
N-doped graphene nanoflakes	167(0.5 A g <sup>-1</sup> )	1.3M N <sup>+</sup> Me <sub>4</sub> TFSI <sup>-</sup>	[24]
Wheat flour	168(0.5 A g <sup>-1</sup> )	1M H <sub>2</sub> SO <sub>4</sub>	[25]
Amitrole	244(0.2 A g <sup>-1</sup> )	6M KOH	[26]
Polyaniline/graphene oxide	206(1 A g <sup>-1</sup> )	6M KOH	[27]
Glucose	223(1 A g <sup>-1</sup> )	6M KOH	[28]
Pueraria	250(0.5 A g <sup>-1</sup> )	6M KOH	[29]
Cigarette filters	263(1 A g <sup>-1</sup> )	6M KOH	[30]
Glucosamine	244(0.5 A g <sup>-1</sup> )	6M KOH	[31]
Chitosan	252(0.5 A g <sup>-1</sup> )	6M KOH	[32]
Carbon nano-cages	260(1 A g <sup>-1</sup> )	6M KOH	[33]
<b>APC</b>	<b>272(0.5 A g<sup>-1</sup>)</b>	<b>6M KOH</b>	<b>This work</b>

## Reference:

- [1] Shang, Z. An, X. Zhang, H. Shen, M. Baker, F. Liu, Y. Liu, L. Yang, J. Cao, H. Xu, Q. Liu, H. Ni, Y. Houttuynia-derived nitrogen-doped hierarchically porous carbon for high-performance supercapacitor. *Carbon*. **2020**;161:62-70.
- [2] Hu, X. Wang, Y. Ding, B. Wu, X. A novel way to synthesize nitrogen doped porous carbon materials with high rate performance and energy density for supercapacitors. *Journal of Alloys and Compounds*. **2019**;785:110-116.
- [3] Yuan, Y. Sun, Y. Feng, Z. Li, X. Yi, R. Sun, W. Zhao, C. Yang, L. Nitrogen-Doped Hierarchical Porous Activated Carbon Derived from Paddy for High-Performance Supercapacitors. *Materials (Basel)*. **2021**:14.
- [4] Kwak, M.-J. Ramadoss, A. Yoon, K.-Y. Park, J. Thiyagarajan, P. Jang, J.-H. Single-Step Synthesis of N-Doped Three-Dimensional Graphitic Foams for High-Performance Supercapacitors. *ACS Sustainable Chemistry & Engineering*. **2017**;5:6950-6957.
- [5] Sahoo, M. K. Rao, G. R. A high energy flexible symmetric supercapacitor fabricated using N-doped activated carbon derived from palm flowers. *Nanoscale Advances*. **2021**;3:5417-5429.
- [6] He, D. Niu, J. Dou, M. Ji, J. Huang, Y. Wang, F. Nitrogen and oxygen co-doped carbon networks with a mesopore-dominant hierarchical porosity for high energy and power density supercapacitors. *Electrochimica Acta*. **2017**;238:310-318.
- [7] Gong, Y. Li, D. Fu, Q. Zhang, Y. Pan, C. Nitrogen Self-Doped Porous Carbon for High-Performance Supercapacitors. *ACS Applied Energy Materials*. **2020**;3:1585-1592.
- [8] Sudhan, N. Subramani, K. Karnan, M. Ilayaraja, N. Sathish, M. Biomass-Derived Activated Porous Carbon from Rice Straw for a High-Energy Symmetric Supercapacitor in Aqueous and Non-aqueous Electrolytes. *Energy & Fuels*. **2016**;31:977-985.
- [9] Zeng, R. Tang, X. Huang, B. Yuan, K. Chen, Y. Nitrogen-Doped Hierarchically Porous Carbon Materials with Enhanced Performance for Supercapacitor. *ChemElectroChem*. **2018**;5:515-522.
- [10] Shen, C. Li, R. Yan, L. Shi, Y. Guo, H. Zhang, J. Lin, Y. Zhang, Z. Gong, Y. Niu, L. Rational design of activated carbon nitride materials for symmetric supercapacitor applications. *Applied Surface Science*. **2018**;455:841-848.
- [11] Dong, D. Zhang, Y. Xiao, Y. Wang, T. Wang, J. Romero, C. E. Pan, W. P. High performance aqueous supercapacitor based on nitrogen-doped coal-based activated carbon electrode materials. *J Colloid*

- Interface Sci.* **2020**;580:77-87.
- [12] Guan, L. Pan, L. Peng, T. Gao, C. Zhao, W. Yang, Z. Hu, H. Wu, M. Synthesis of Biomass-Derived Nitrogen-Doped Porous Carbon Nanosheets for High-Performance Supercapacitors. *ACS Sustainable Chemistry & Engineering*. **2019**;7:8405-8412.
- [13] Ghanashyam, G. Jeong, H. K. Synthesis of plasma treated nitrogen-doped graphite oxide for supercapacitor applications. *Journal of Energy Storage*. **2019**:26.
- [14] Maria Sundar Raj, F. R. Jaya, N. V. Boopathi, G. Kalpana, D. Pandurangan, A. S-doped activated mesoporous carbon derived from the *Borassus flabellifer* flower as active electrodes for supercapacitors. *Materials Chemistry and Physics*. **2020**:240.
- [15] Ni, G. Qin, F. Guo, Z. Wang, J. Shen, W. Nitrogen-doped asphaltene-based porous carbon fibers as supercapacitor electrode material with high specific capacitance. *Electrochimica Acta*. **2020**:330.
- [16] Gong, Y. Chen, R. Xu, H. Yu, C. Zhao, X. Sun, Y. Hui, Z. Zhou, J. An, J. Du, Z. Sun, G. Huang, W. Polarity-assisted formation of hollow-frame sheathed nitrogen-doped nanofibrous carbon for supercapacitors. *Nanoscale*. **2019**;11:2492-2500.
- [17] Lu, H. Liu, S. Zhang, Y. Huang, Y. Zhang, C. Liu, T. Nitrogen-Doped Carbon Polyhedra Nanopapers: An Advanced Binder-Free Electrode for High-Performance Supercapacitors. *ACS Sustainable Chemistry & Engineering*. **2019**;7:5240-5248.
- [18] Sun, L. Tian, C. Li, M. Meng, X. Wang, L. Wang, R. Yin, J. Fu, H. From coconut shell to porous graphene-like nanosheets for high-power supercapacitors. *Journal of Materials Chemistry A*. **2013**:1.
- [19] Li, Y.-T. Pi, Y.-T. Lu, L.-M. Xu, S.-H. Ren, T.-Z. Hierarchical porous active carbon from fallen leaves by synergy of  $K_2CO_3$  and their supercapacitor performance. *Journal of Power Sources*. **2015**;299:519-528.
- [20] Jiang, D. Li, C. Yang, W. Zhang, J. Liu, J. Fabrication of an arbitrary-shaped and nitrogen-doped graphene aerogel for highly compressible all solid-state supercapacitors. *Journal of Materials Chemistry A*. **2017**;5:18684-18690.
- [21] Li, L. Zhong, Q. Kim, N. D. Ruan, G. Yang, Y. Gao, C. Fei, H. Li, Y. Ji, Y. Tour, J. M. Nitrogen-doped carbonized cotton for highly flexible supercapacitors. *Carbon*. **2016**;105:260-267.
- [22] Wu, K. Liu, Q. Nitrogen-doped mesoporous carbons for high performance supercapacitors. *Applied Surface Science*. **2016**;379:132-139.
- [23] Wang, X. Ding, Y. Lu, H. Chen, F. Zhang, N. Ma, M. Chemoselective solution synthesis of pyrazolic-

- structure-rich nitrogen-doped graphene for supercapacitors and electrocatalysis. *Chemical Engineering Journal*. **2018**;347:754-762.
- [24] Arkhipova, E. A. Ivanov, A. S. Maslakov, K. I. Savilov, S. V. Nitrogen-doped mesoporous graphene nanoflakes for high performance ionic liquid supercapacitors. *Electrochimica Acta*. **2020**:353.
- [25] Yu, P. Wang, Q. Zheng, L. Jiang, Y. Construction of Ultrathin Nitrogen-Doped Porous Carbon Nanospheres Coated With Polyaniline Nanorods for Asymmetric Supercapacitors. *Front Chem*. **2019**;7:455.
- [26] Śliwak, A. Grzyb, B. Díez, N. Gryglewicz, G. Nitrogen-doped reduced graphene oxide as electrode material for high rate supercapacitors. *Applied Surface Science*. **2017**;399:265-271.
- [27] Wang, W.-D. Lin, X.-Q. Zhao, H.-B. Lü, Q.-F. Nitrogen-doped graphene prepared by pyrolysis of graphene oxide/polyaniline composites as supercapacitor electrodes. *Journal of Analytical and Applied Pyrolysis*. **2016**;120:27-36.
- [28] Zhang, W. Ren, Z. Ying, Z. Liu, X. Wan, H. Activated nitrogen-doped porous carbon ensemble on montmorillonite for high-performance supercapacitors. *Journal of Alloys and Compounds*. **2018**;743:44-51.
- [29] Han, X. Jiang, H. Zhou, Y. Hong, W. Zhou, Y. Gao, P. Ding, R. Liu, E. A high performance nitrogen-doped porous activated carbon for supercapacitor derived from pueraria. *Journal of Alloys and Compounds*. **2018**;744:544-551.
- [30] Xiong, Q. Bai, Q. Li, C. Li, D. Miao, X. Shen, Y. Uyama, H. Nitrogen-doped hierarchical porous carbons from used cigarette filters for supercapacitors. *Journal of the Taiwan Institute of Chemical Engineers*. **2019**;95:315-323.
- [31] Xu, Z. Chen, J. Zhang, X. Song, Q. Wu, J. Ding, L. Zhang, C. Zhu, H. Cui, H. Template-free preparation of nitrogen-doped activated carbon with porous architecture for high-performance supercapacitors. *Microporous and Mesoporous Materials*. **2019**;276:280-291.
- [32] Deng, X. Zhao, B. Zhu, L. Shao, Z. Molten salt synthesis of nitrogen-doped carbon with hierarchical pore structures for use as high-performance electrodes in supercapacitors. *Carbon*. **2015**;93:48-58.
- [33] Xie, K. Qin, X. Wang, X. Wang, Y. Tao, H. Wu, Q. Yang, L. Hu, Z. Carbon nanocages as supercapacitor electrode materials. *Adv Mater*. **2012**;24:347-52.